N92-29816

SIMS CHEMICAL ANALYSIS OF EXTENDED IMPACT FEATURES FROM THE TRAILING EDGE PORTION OF EXPERIMENT AO187-2

Sachiko Amari, John Foote, Charles Simon,
Pat Swan, Robert M. Walker, Ernst Zinner
McDonnell Center for the Space Sciences
Washington University
One Brookings Drive
Saint Louis MO 63130-4899 USA
Phone: 314-889-6257, Fax: 314-889-6219

Elmar K. Jessberger, Gundolf Lange, Frank Stadermann
Max-Planck-Institut für Kernphysik
Postfach 103980
6900 Heidelberg, Germany

SUMMARY

One hundred capture cells from the trailing edge, which had lost their cover foils during flight, were optically scanned for extended impact features caused by high velocity projectiles impinging on the cells while the foils were still intact. Of 53 candidates, 24 impacts were analyzed by secondary ion mass spectrometry for the chemical composition of deposits. Projectile material was found in all impacts, and at least 75% of them appear to be caused by interplanetary dust particles. Elemental ratios are fractionated, with refractory elements enriched in the impacts relative to interplanetary dust particles collected in the stratosphere. Although this could be due to systematic differences in the compositions, a more likely explanation is volatility fractionation during the impact process.

INTRODUCTION

The main scientific objective of LDEF experiment AO187-2 was the collection of interplanetary dust material in space and its elemental and isotopic analysis in the laboratory. Although interplanetary dust collected in the upper atmosphere has been available for analysis in terrestrial laboratories for more than a decade (e.g., refs. 1, 2), the stratospheric collection undoubtedly is biased since not all extraterrestrial dust particles entering the Earth's atmosphere are collected. For example, cometary dust particles have, on average, a higher velocity and are therefore expected to have a much smaller survival probability of atmospheric entry than dust grains originating from asteroids (refs. 3, 4). In order to obtain an unbiased sample of interplanetary dust it is necessary to collect this material in space. LDEF provided an unprecedented opportunity for this purpose, combining large collecting areas with long exposure times.

A fundamental problem for the collection of interplanetary dust material is the high relative velocity of dust grains (10-15 km/sec). At these high velocities a major fraction of projectile material is lost upon impact with most collection surfaces. A viable compromise is to forgo the collection of solid dust grains

or fragments thereof and to concentrate on the collection of their atoms in capture cells. LDEF carried several capture cell experiments (AO023, AO138-2); the principle of AO187-2 is shown in Figure 1. A target plate is covered by a thin foil separated by a small distance. A high velocity dust grain of sufficient size penetrates the foil and normally is disrupted in the process, spreading out into a shower of debris. This shower impacts the target plate, being further disrupted, melted and vaporized. The projectile material ejected from the impact zone is collected on the backside of the foil and then analyzed.

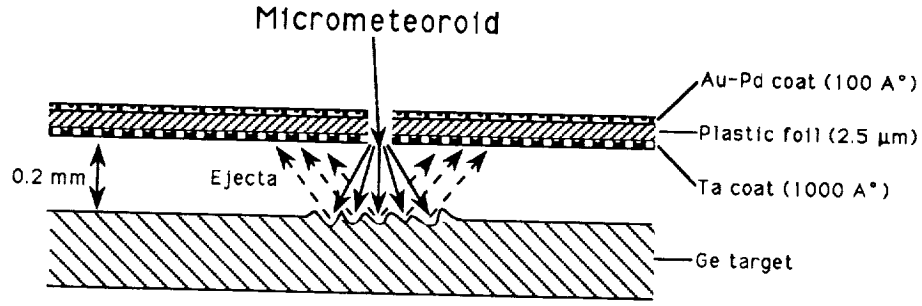

Figure 1. Principle of capture cell of experiment AO187-2.

A series of simulation experiments on laboratory dust accelerators proved this concept to be viable (refs. 5-7): projectile material could indeed be collected on the surface of the target plate and the backside of the foil and its elemental and isotopic composition measured. Since the collected material exists as a thin surface deposit, secondary ion mass spectrometry (SIMS) with its extremely high surface sensitivity proved to be the best-suited analysis technique. In fact, since one of the main objectives of the experiment was the isotopic measurement of dust material, AO187-2 was originally conceived and optimized for SIMS analysis. The choice of materials was largely determined by the requirements for extreme purity and high ion yields for SIMS analysis.

EXPERIMENT DESCRIPTION AND PRELIMINARY ASSESSMENT

LDEF experiment AO187-2 consisted of 237 capture cells, each 8.6 × 9.4 cm in size. A capture cell in turn consisted of four polished high purity germanium plates, 42 × 39 × 0.5 mm, covered with a plastic foil separated from the Ge plate by 200µm. The Ge plates were glued to an Al base plate, the 2.5 µm thick mylar cover foil was coated with 1300 Å of Ta on the backside and 100 Å of Au-Pd on the front side. Ta was chosen to optimize the SIMS analysis of deposited projectile material; Au-Pd was chosen to protect the foil from erosion by atomic oxygen in the residual atmosphere impinging on the leading edge of LDEF (refs. 8, 9).

The capture cells occupied locations on three different trays. A full tray, E8, on the leading edge contained 120 cells, 77 cells were mounted on tray E3 and 40 took up a third of tray C2, both on the trailing edge. By having capture cells on both the leading and the trailing edge, the experiment was expected to obtain information on both interplanetary dust and man-made space debris in low Earth orbit.

After the return of LDEF it was found that all capture cells on the leading edge tray E8 had lost their plastic-metal foils and only 12 cells on the trailing edge had retained them, 11 on tray E3 and one on tray C2. Four capture cells from tray E8 and 5 cells without foil from tray E3 were shipped to Messerschmitt-Bölkow-Blohm in Germany; the rest of the cells went to Washington University. At present we do not know why the foils failed or when this happened. The fact that 12 intact cells were found on the trailing

edge indicates that the failure mechanism probably was not the same for the two locations. Atomic oxygen erosion starting from impact holes or spots with damages in the protective metal coating is a likely cause for the complete failure of the cells on the leading edge of tray E8. The capture cells on the trailing edge, however, never were exposed to an atomic oxygen flux. A combination of embrittlement by solar UV and stress failure under thermal cycling is a possible cause but this hypothesis has to be substantiated by future tests. If we assume that the failure of foils on the trailing edge is an exponential function of time, 67% of the cells would have been still intact after one year, the nominal deployment duration for LDEF.

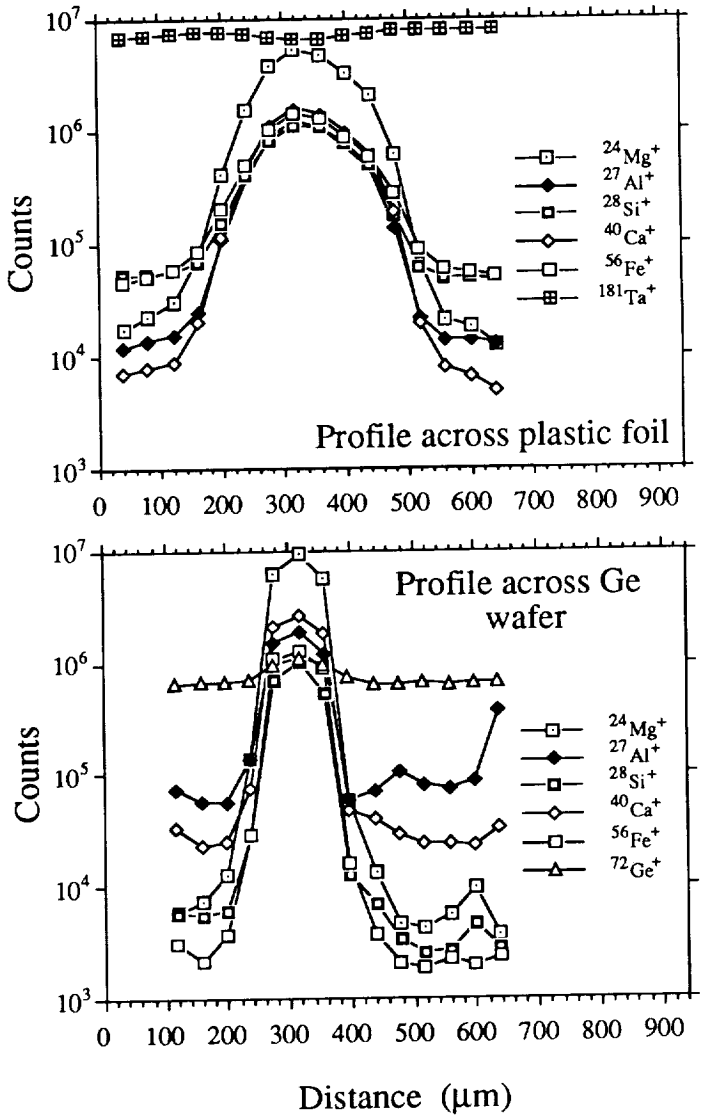

Figure 2. Lateral elemental profiles across plastic foil and Ge wafer of the same simulation impact.

Preliminary optical microscope examination of cells from the trailing edge that had lost their cover foils (bare cells) showed numerous "extended impact features" as well as typical hypervelocity impact craters produced by direct hits. The extended impact features resembled laboratory simulation impacts produced by projectile material that had penetrated plastic foils and had suffered disruption. Apparently, the extended impact features found on the bare LDEF cells were produced by high velocity impacts onto the cells while the foils were still intact. Since prior simulation studies (ref. 7) had shown that extended impacts on the Ge plates contained sufficient projectile material for chemical and isotopic analysis by SIMS (Fig. 2), we first concentrated our analysis effort on the extended impacts found in the bare LDEF capture cells from the trailing edge (trays E3 and C2). These were the best candidates to contain impacts of interplanetary dust particles with a minimum contribution from orbital debris. Furthermore, foil survival on 10% of trailing edge cells compared to none on the leading edge indicated that even foils that failed lasted, on average, longer on the trailing than the leading edge.

All 100 bare capture cells from E3 and C2 in our possession were optically scanned for impact features. During the scanning we developed criteria for the classification of these impacts and for the selection of candidates for SIMS analysis. All selected candidates were further documented in a scanning electron microscope (SEM). To date, a subset of these candidates has been analyzed by SIMS for the chemical composition of deposited material.

OPTICAL AND SEM CHARACTERIZATION

All bare cells in our possession from the trailing edge, 61 from tray E3 and 39 from tray C2, were scanned under oblique illumination in an optical stereo microscope with a 12× objective and 20× eyepiece. The Al plates with the Ge wafers were mounted on a scanning stage whose position could be read with an accuracy of 50 μm. The wafers were scanned a row (of 6.0 mm width) at a time. Recorded were the locations of impact features and their sizes and other interesting properties. Among the impacts we distinguished between "craters" and "extended impacts." Since Ge is very brittle, craters produced by direct hits (i.e. without penetration of a foil) are not likely to contain much residual material from the projectile and this expectation was confirmed by subsequent analysis. Figure 3 shows a SEM image of a crater.

The extended impacts are the most interesting since they are expected to contain projectile material. They range from 200 μm to 4000 μm in diameter and were divided into two categories, A and B. Category A comprises larger impacts that are expected to contain deposits and are high priority candidates for SIMS analysis. Category B impacts are smaller and will be studied last. Features that could not be recognized with certainty as extended impacts in the optical microscope were classified as "possible extended impacts (Category A or B)," and were examined in more detail in the SEM.

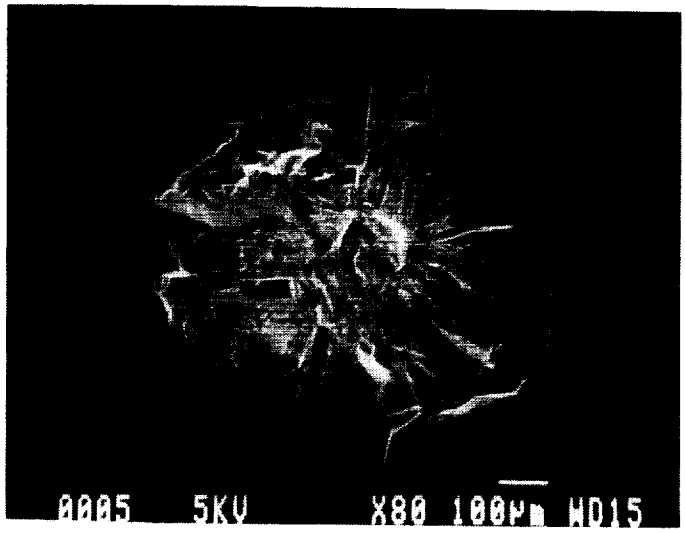

Figure 3. Crater produced by hypervelocity impact onto Ge wafer without cover foil.

Extended impacts of category A and B were further classified into four sub-categories according to their morphology.

1) Craters surrounded by deposits (CD).
2) Ring-shaped features (RI).
3) Sprays (SP).
4) Spider webs (SW).

Figure 4 shows SEM micrographs of one of each morphology. The more detailed SEM images revealed that in many cases an extended impact showed features of different categories (e.g. a crater surrounded by deposits also had spider web features).

Scanning in the SEM was performed with a twofold purpose:

a) To check all features that had been classified as "possible extended impacts" during the initial optical scanning to determine which of them are true "extended impacts."
b) To document in detail all extended impacts to be selected for SIMS analysis.

Table 1 gives a summary of the results of the optical scanning. So far, 98 of 157 possible extended impacts have been examined in the SEM and five of them have been reclassified as extended impacts (2 CD, 3 RI).

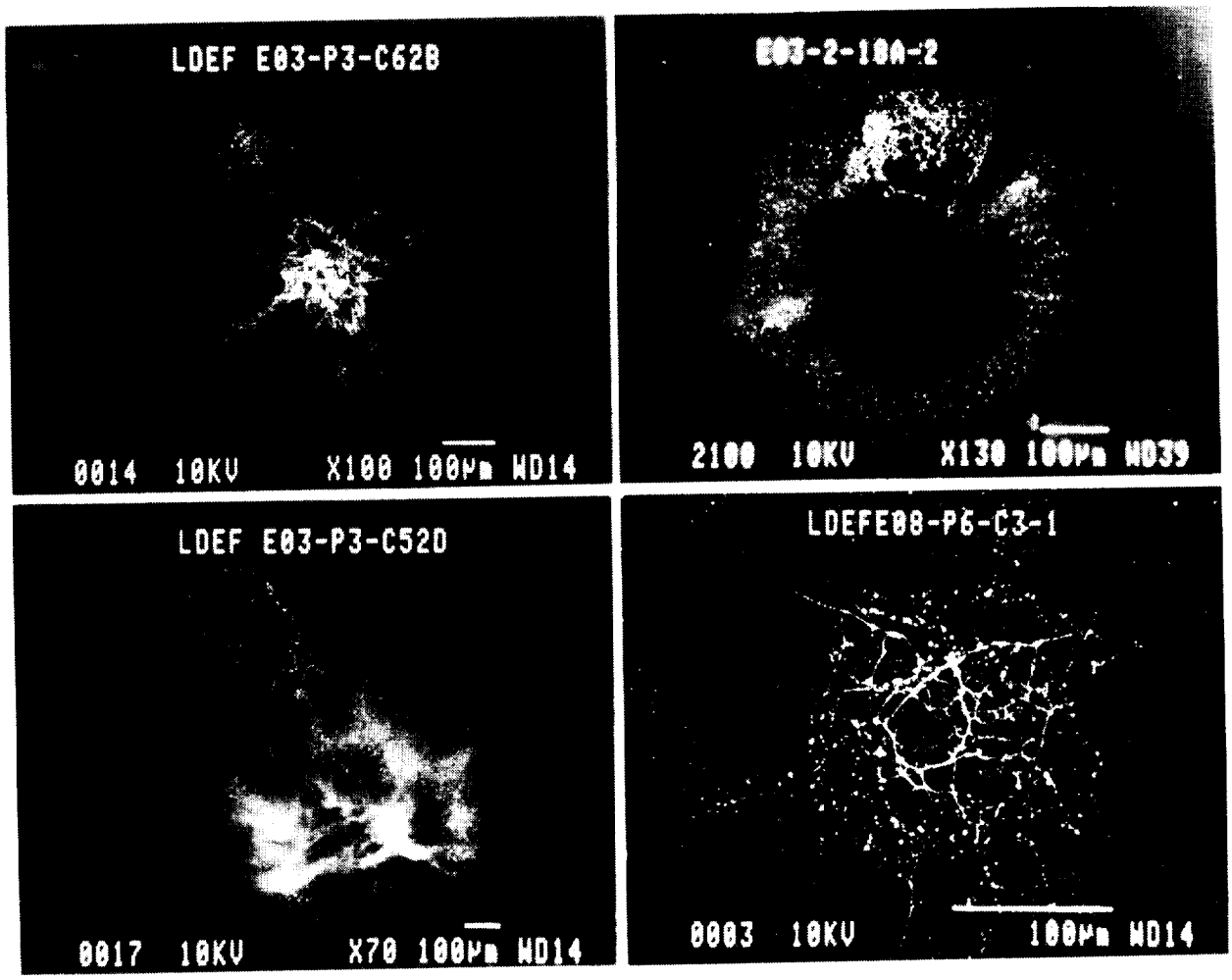

Figure 4. Morphologies of extended impacts: Craters surrounded by deposits (upper left), ring (upper right), spray (lower left), and spider web (lower right).

Table 1. Classification of impacts on bare capture cells from the trailing edge

Extended Impacts		CD	RI	SP	SW	Total
	A	14	8	8	23	53
	B	5	42	94	14	155
Possible Extended Impacts	A					157
	B					177
Craters						203

During the SEM documentation of extended impacts energy dispersive x-ray (EDX) spectra were obtained in most cases, especially if fragments were observed in the area of the impact. However, fragments usually turned out to be pieces of the Ta coating of the mylar foil or other apparent contaminants. Generally it was not possible to detect any elements besides Ge. An exception was Si which is present in quantities detectable by EDX on all Ge wafers

from the leading and trailing edge. The Si concentrations on the wafers are non-uniform, being highest on the edges and lowest in the middle of the Ge plates. The most likely cause for this ubiquitous Si background is outgassing or migration of the RTV used to bond the Ge onto the Al substrate (in spite of the space rating of this material). This unfortunate circumstance deprived us (with a few exceptions) of the opportunity to measure one of the most important cosmochemical elements in the projectile deposits.

A comparison of the extended impact features on Ge from the trailing edge and simulation impacts produced on the same foil-target assembly in the Munich plasma dust accelerator (refs. 10, 11) at velocities between 3 and 8 km/sec shows significant differences. The LDEF impacts are, on average, larger and much more irregular. The simulation impacts usually are spider webs with a high degree of rotational symmetry or ring-shaped features with typical diameters of 100-200μm. There are two possible explanations for the large irregular impact features found on the Ge plates from the trailing edge. One is that many impacts were produced by projectiles that hit the capture cells at oblique angles. The second is that the foil had already been damaged and some of it had curled up when the impact occurred, leading to a much more complex foil-target geometry than for the simulation impacts, which were produced at normal incidence.

SIMS ANALYSIS OF EXTENDED IMPACTS

For SIMS analysis the Ge wafers were cut into smaller pieces containing extended impacts of interest. This was done by a newly developed laser cutting technique, which avoids any of the contamination incurred by sawing. A CW YAG laser beam of 1.06 μm wavelength was focussed onto the rough backside of the Ge wafer (this side has a higher absorption at this wavelength than the polished front side). At a power of 50 W a short scan across the wafer at a speed of 5 cm/sec was sufficient to cause a break along the scanned line most of the time. Sometimes the wafers broke along other defects or along crystal boundaries; however, in all such cases intact pieces of appropriate size could be obtained for ion probe analysis.

To date 24 of a total 53 extended impacts of category A have been analyzed by SIMS for the chemical composition of projectile deposits. All measurements were made on the Washington University ion microprobe, a modified CAMECA IMS 3f instrument. For chemical analysis we obtained lateral scanning profiles across the impact features. For this purpose at each analysis point an O^- primary ion beam of 1-2 nA current was rastered over an area of 40μm×40μm. As the primary ion beam sputtered away the surface of the analyzed sample layer by layer, positive secondary ions selected from the central portion of the rastered area by a beam aperture were mass analyzed in a double focussing magnetic mass spectrometer and counted by an electron multiplier detection system.

Multi-element depth profiles are obtained by cycling the mass spectrometer through a set of isotopic masses of the selected elements. After analysis of a given area consisting of 40 cycles the sample is stepped (by 40 or 50 μm) to the next area. Fig. 5a shows a SEM micrograph of an extended impact after two step-scanning analyses were made on this sample. The individual depth profiles were integrated over cycles 4 to 40 to obtain lateral profiles in the form of the integrated secondary ion intensity as a function of lateral distance. The first three cycles were not included in order to reduce the effect of surface contamination and because a variety of artifacts are encountered during sputtering of the very surface.

Ion signals associated with material from the impacts could be detected in all 24 analyzed impact areas but large variations were observed between individual impacts. For example, the ratio of the maximum $^{24}Mg^+$ signal to the $^{72}Ge^+$ signal for an individual lateral intensity profile varies over almost 5 orders of magnitude.

The ideal case is shown by the profile of Fig. 5b, which corresponds to the top scan in Fig. 5a. This scan has well defined maxima for all the isotopic masses measured except for $^{72}Ge^+$. It is one of the few cases where the $^{28}Si^+$ also displays a clear maximum above background; the latter, however, is much higher for this element than for all the others (since the yield of positive secondary ions is less for Si than for Mg, Al, Ca and Fe; this discrepancy in the background is actually much larger than is indicated by the plot of Fig. 5b). The profile across impact EO3-2-19C-1 is also one of the few which gives a clear signal for Ni^+ at mass 60. The reason is that the signals associated with impact deposits are relatively high compared to the Si background. In most other cases, these signals are much lower so that the molecular interference from $^{28}SiO_2^+$ dominates at mass 60.

In order to obtain elemental abundances, the ion yields of different elements as well as the isotopic abundances have to be taken into account. Table 2 gives sensitivity factors S relative to Si so that

$$\frac{C_{El}}{C_{Si}} = \frac{I_{El}}{I_{Si}} / S_{El/Si}$$

where C are the atomic concentrations and I are the secondary ion signals (corrected for isotopic abundances) for the element of interest and the standard element Si. The sensitivity factors were determined from measurements on four different glasses (Lunar Analog Glass, Solar Glass NTR-1, Window Glass and Dunite Glass).

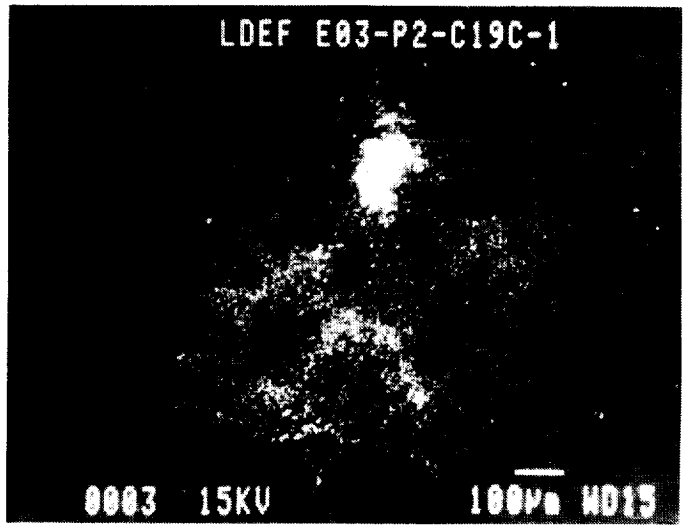

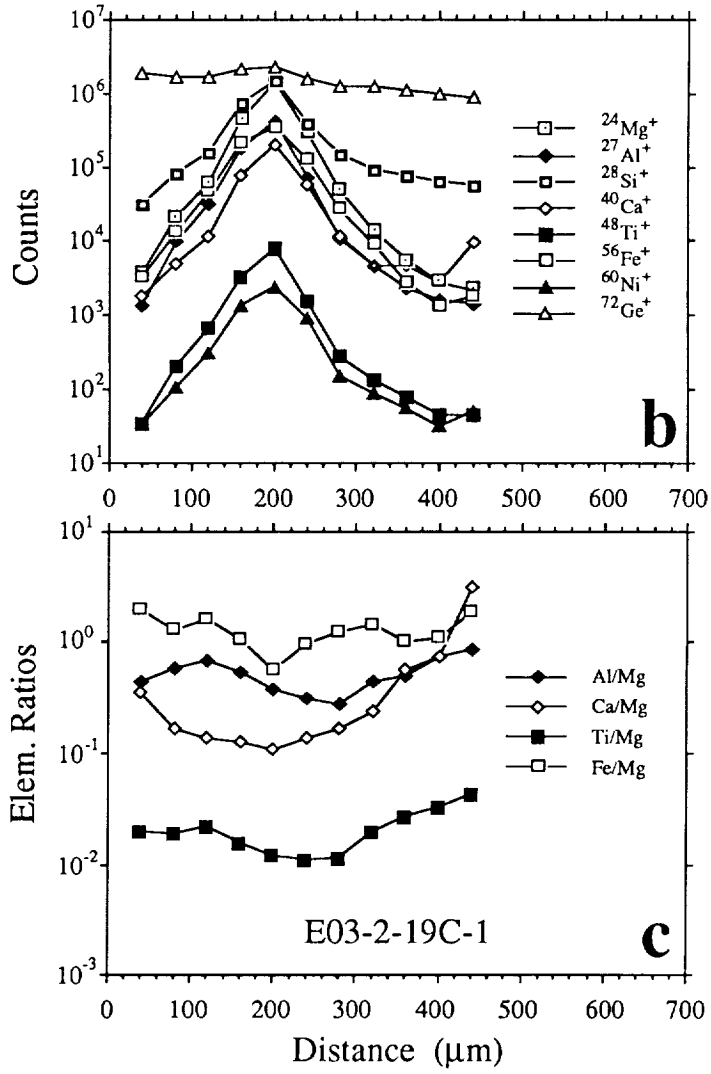

Figure 5. Ion microprobe elemental scans across impact E03-2-19C-1. Profiles in b and c correspond to the upper scan in the SEM micrograph.

Because of the problems with Si contamination of the Ge wafers we normalized the lateral intensity profiles to Mg by applying the relative sensitivity factors of Table 2. The resulting profiles of atomic elemental ratios are shown in Fig. 5c. One feature typical for almost all impacts is apparent from this figure: elemental ratios change across a lateral profile or, in other words, the deposits from the impact have different spatial distributions for different elements. For example, the Fe/Mg ratio has a minimum at lateral position 200 μm, where all the elements show a maximum, and changes by more than a factor of two 80-100 μm to the left and right of the maximum position. This can also be seen directly in Fig. 5b where the $^{56}Fe^{+}$ profile is slightly wider between positions 100 μm and 300 μm than the $^{24}Mg^{+}$ profile. This means that Fe apparently is distributed over a wider area than Mg.

Table 2. Secondary ion sensitivity factors relative to Mg.

Element	S
Na	3.28 ± .15
Al	0.77 ± .09
Si	0.13 ± .01
Ca	1.47 ± .24
Ti	0.50 ± .04
Cr	0.38 ± .15
Mn	0.51 ± .09
Fe	0.47 ± .07

Most impacts show even more complex distributions of the deposited elements. An example is impact CO2-1-20D-2 whose SEM micrograph after SIMS analysis is shown in Fig. 6a. The corresponding lateral intensity profile is displayed in Fig. 6b. There are several interesting observations to be made on this impact, which was classified as CD (crater with deposits). The first is that the ion signals of elements apparently deposited from the projectile (Mg, Ca, Fe) are much lower in the crater itself (dip in the middle of the profile) than in surrounding areas. Secondly, the concentrations of Mg and Fe are much higher to the left of the crater than to the right, although on the SEM micrograph the area to the right shows much more "structure" in the impact. The reason for this apparent paradox is that what is "seen" in the SEM is mostly damage to the Ge surface by high-velocity debris from the impact, which, however, contains only little deposited material, while the deposits themselves are not seen in the SEM. Finally, in this impact different elements have very different spatial distributions: the $^{56}Fe^{+}$ signal is higher than the $^{40}Ca^{+}$ signal to the left of the crater, but lower to the right. It is likely that such changing elemental ratios reflect heterogeneities in the chemical composition of the original projectile.

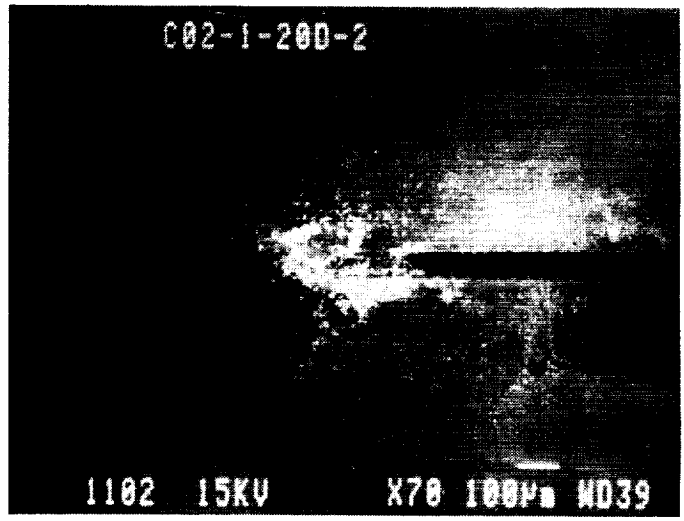

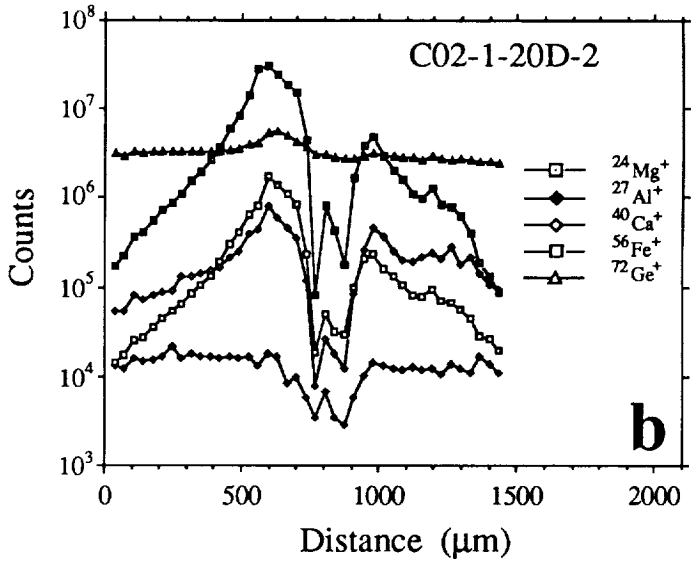

Figure 6. Ion probe scan across impact C02-1-20D-2, a crater with associated deposits.

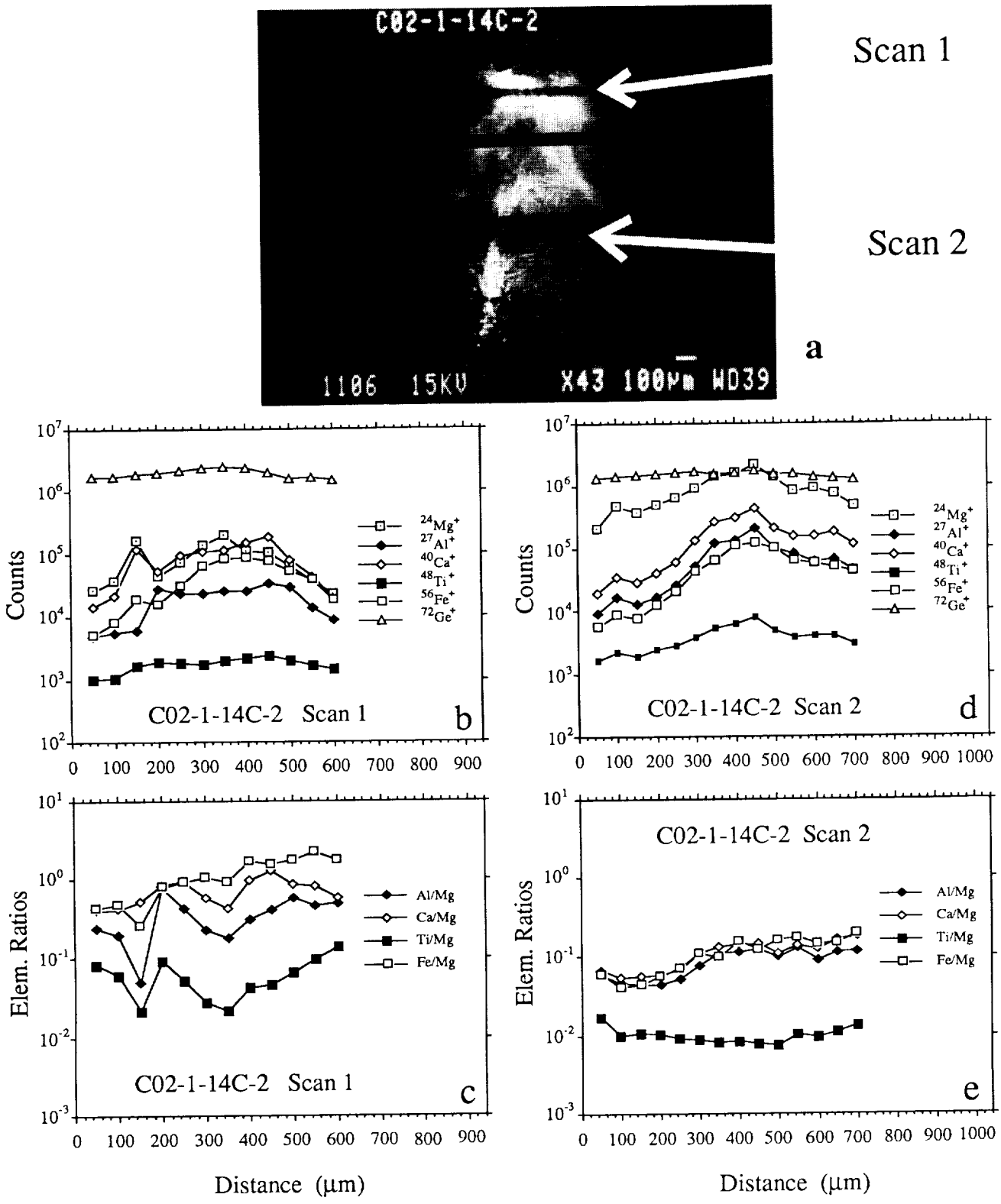

Figure 7. Two ion microprobe elemental scans across the same extended impact.

An even more extreme example of elemental heterogeneity is shown in Fig. 7, depicting a large extended impact (C02-1-14C-2) classified as SW (spider web) together with the results of two lateral scans (the short scans in the SEM micrograph). Not only do the absolute concentrations differ between the two scans (Fig. 7b,d) but there are also large differences in the elemental ratios (Fig.7c,e).

The non-uniform distribution of different elements in the deposition area of a given extended impact makes it difficult to obtain average elemental ratios. As a compromise we have taken elemental ratios determined at the maximum of the $^{24}Mg^{+}$ signal for a given scan. Histograms of these elemental ratios are plotted in Fig. 8 together with histograms of the same ratios measured by SIMS on individual stratospheric dust particles of probable extraterrestrial origin (ref. 12). Chondritic compositions are indicated for reference. The ratios measured in projectile deposits on the LDEF Ge wafers not only show much wider

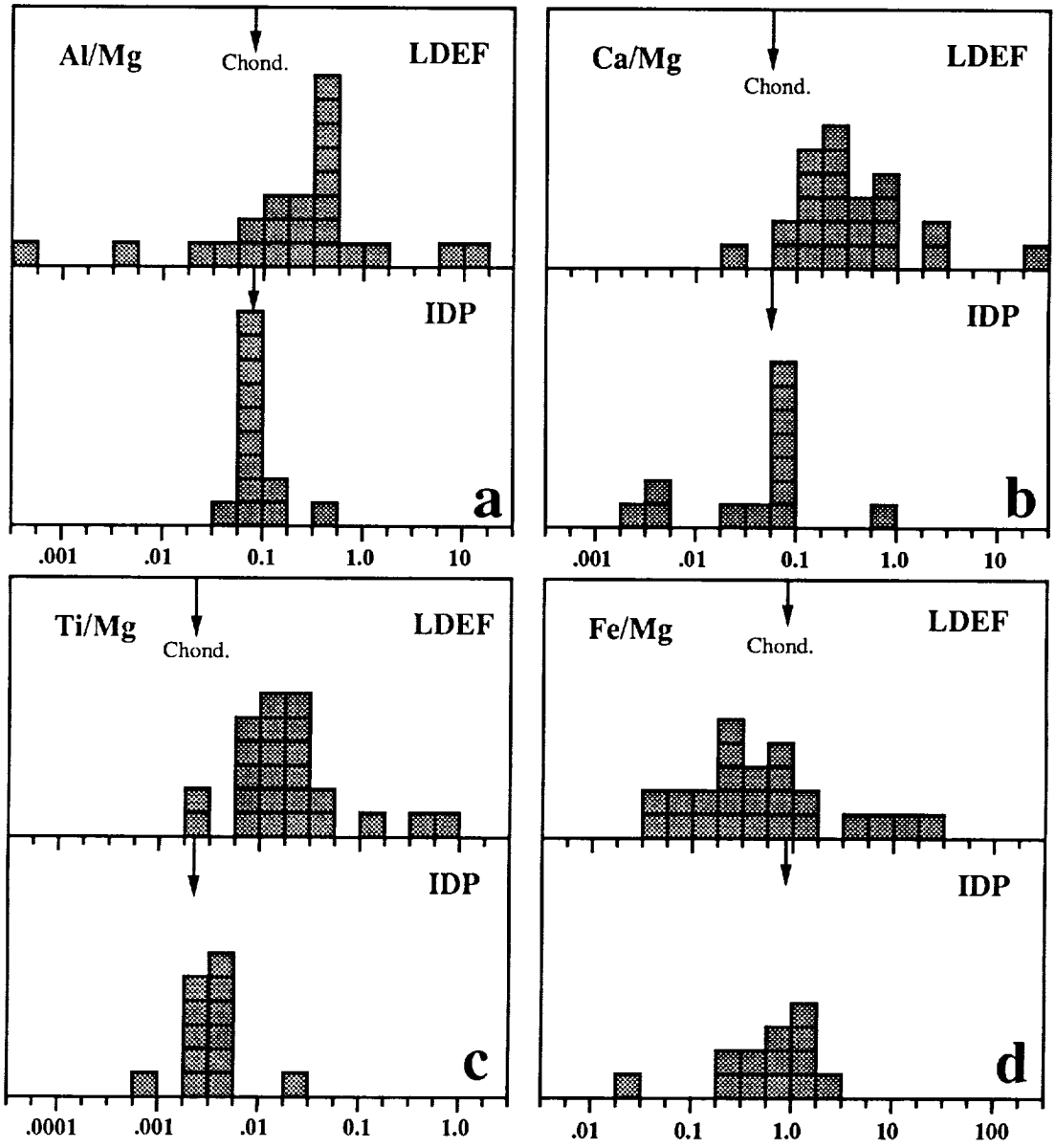

Figure 8. Histograms of elemental ratios in LDEF deposits and interplanetary dust particles.

distributions than those of IDPs but the mean of the distributions are systematically shifted relative to one another. This shift is toward lower values for Fe/Mg but toward higher values for the other three ratios, Al/Mg, Ca/Mg, and Ti/Mg.

There are at least two explanations for these differences. The first is simply that the particles whose material was collected on the Ge wafers on LDEF have chemical compositions that differ significantly from those of IDPs collected in the stratosphere. The second is that the impact process caused strong fractionation between the elements so that the compositions of the deposits do not accurately reflect those of the projectiles. One reason the particles that impacted LDEF have compositions different from IDPs could be that a major portion of them are not interplanetary dust but man-made debris. This, however, is unlikely in our case. First, collection on the trailing edge discriminates to a large extent against orbital debris. Furthermore, Mg is the dominant element in most impacts compared to Fe, Al, Ca and Ti. This is not expected for most man-made debris in orbit, which in this size range is presumably dominated by Al-oxide particles from the exhaust of solid fuel rockets. Moreover, we did not detect any impacts that contain primarily Al (Fig. 9).

Before we consider the possibility of differences in the chemical composition of interplanetary dust particles collected on LDEF and in the stratosphere, we have to discuss elemental fractionation during the impact process. There is evidence for such fractionation from simulation impacts onto the same foil/Ge wafer targets as flown on LDEF. The analysis of 12 extended impacts on the Ge produced by Lunar Analog Glass and Solar Glass showed fractionation between Mg and the other elements in the deposits with average fractionation factors relative to Mg of 0.28 for Fe, 0.58 for Si, 1.60 for Al, 1.95 for Ti and 2.41 for Ca. A fractionation factor smaller than one means that, compared to the projectile, less of the element is found in the deposition area than Mg and the

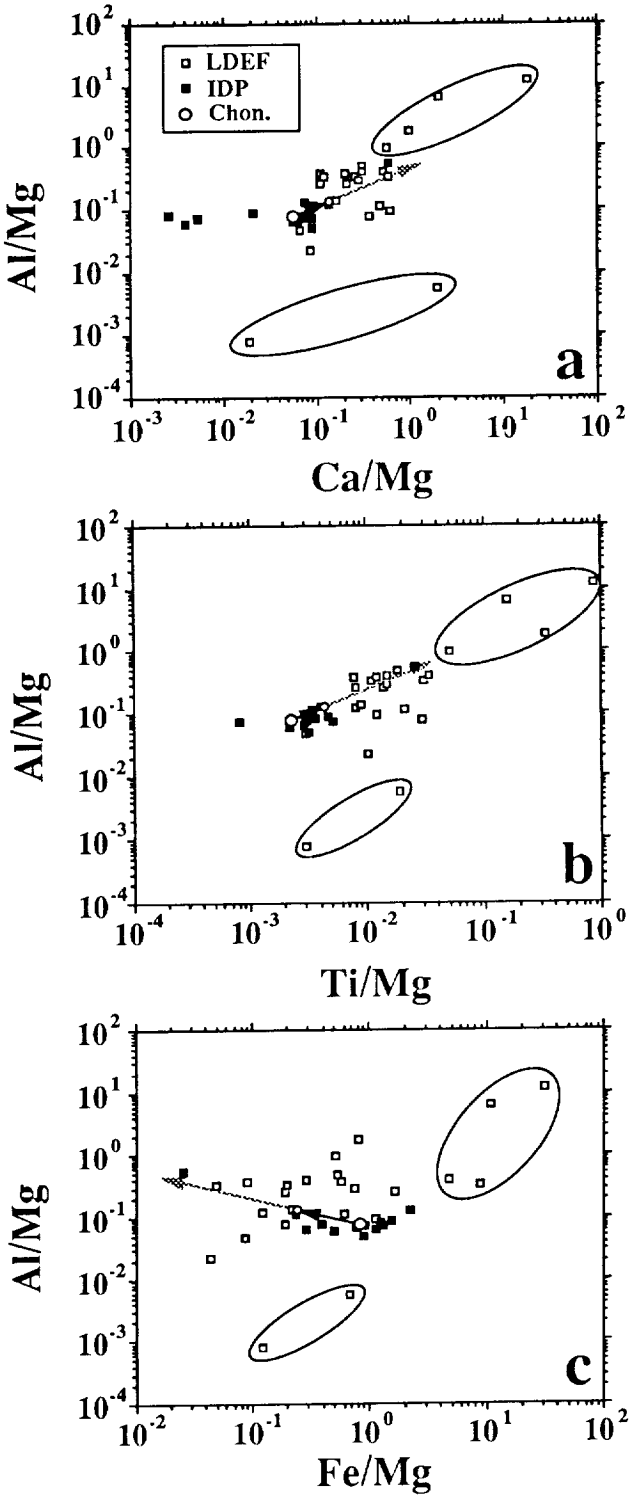

Figure 9. Scatter plots of elemental ratios in LDEF impact deposits and in interplanetary particles. Also shown are chondritic ratios, the elemental fractionations determined from simulation impacts (solid arrows) and the extension of these fractionations (light arrows).

opposite is the case for fractionation factors greater than one. We note that elemental fractionations are related to the relative volatilities of the elements during high temperature evaporation and condensation: the elements Fe and Si are more volatile than Mg and are depleted in the deposits relative to Mg while Al, Ca and Ti are more refractory and are enhanced relative to Mg.

During the impact apparently a large part of the projectile either melts or evaporates. Elements with different volatilities behave differently during this process. More volatile elements such as Fe are almost completely vaporized and expand into a larger volume before they condense onto the Ge and foil surfaces. More refractory elements, on the other hand, either remain in the melt or, if they evaporate, condense sooner and therefore onto a more limited area. Except for the (small) fraction that escapes through the penetration hole, all of the projectile material is retained inside the capture cell but some (preferentially the more volatile elements) is distributed over such a large area that it is lost in the background. For example, if the material of a 10μm projectile is spread out over an area of 1 mm diameter, its thickness is only 2.5 atomic monolayers, only 1/6 of a monolayer for the 4 mm largest observed extended impact.

Figure 9 shows scatterplots of pairs of elemental ratios for the LDEF deposits and individual IDPs. Also shown are the chondritic compositions and the shifts in these compositions if this material experienced the same elemental fractionations as those determined in the impact simulation experiments. The differences between most LDEF deposit compositions and the IDP compositions qualitatively agree with the shifts expected from fractionation during impacts, except that the differences are much larger than the shifts predicted from fractionation. However, we cannot exclude the possibility that elemental fractionations are actually much higher during impacts on LDEF than during simulation impacts. We have already pointed out that the LDEF extended impacts on the Ge are generally much larger than the simulation impacts from which the above fractionation factors were derived. It is reasonable to expect that elemental fractionation factors increase with the size of the extended impact feature. However, the uncertainty in this extension, the extremely irregular structure of most impact features and the fact that the fractionation factors undoubtedly depend on the composition of the projectile itself set a fundamental limit to the extent to which the projectile composition can be derived from the measured composition of the deposits.

Tentatively we can identify most of the LDEF impacts as being caused by cosmic dust particles. Six data points in Fig. 9 fall completely outside of the predicted trend due to elemental fractionation (they are enclosed in ellipses in the Figures). Four of them have extremely high Al/Mg, Ti/Mg and Ca/Mg but also very high Fe/Mg and are likely to be contaminants. The other two have low Al/Mg ratios. This leaves us with 18 (75%) impacts of likely interplanetary origin. While some of them have only little deposited material, some have plenty of it (see, e.g., Figs. 5, 6 and 7) and are candidates for future isotopic measurements. We also plan additional chemical analyses of elements that can easily be detected as negative secondary ions such as C, O, and S.

CONCLUSIONS

1. SIMS analyses of 24 extended impact features on Ge surfaces from "bare" trailing edge capture cells show evidence for projectile material in all of them, but there are large variations in the detected concentrations.

2. The deposits are very thin and cannot be detected by EDX analysis; SIMS appears to be the only method to detect them.

3. Elemental concentrations on the Ge do not correlate exactly with impact features seen in the SEM images; the latter are dominated by damaged regions which contain little projectile material.

4. There is evidence for large variations of elemental ratios within a given extended impact, indicating a heterogeneous chemical composition of the projectile.

5. Comparison with simulation impacts indicates that most LDEF impacts analyzed by SIMS were caused by small (<10μm) projectiles.

6. At least 75% of the analyzed impacts appear to be from interplanetary dust particles but elemental ratios scatter much more than those measured in IDPs collected in the stratosphere.

7. Elemental ratios are also shifted compared to IDPs, with refractory elements being relatively enriched. These shifts are likely to be due to elemental fractionation effects caused by evaporation during the impact process, but systematic differences between IDPs and LDEF impacts cannot be ruled out.

FUTURE WORK

Fractionation effects should be much less pronounced in isotopic ratios than in elemental ratios. Moreover, such effects will not obscure large anomalies of specific isotopes (if present) such as those found by us in studies of interstellar grains isolated from meteorites (ref. 13). As a consequence, future work will concentrate on isotopic measurements in those impacts that have been found in our initial survey to contain sufficient amounts of projectile material.

We have also refrained from studying the 12 intact (precious) capture cells until our handling and analysis techniques had been perfected on the more abundant, extended impacts found in the bare cells. The analysis of the intact cells should provide a critical test of the usefulness of our capture cell concept for future space flight experiments.

Detailed studies of impacts on the cells from the leading edge tray E8 should yield data relevant to the orbital debris problem. The ratios of extended impacts to single craters in these cells should allow us to determine when the plastic cover foils failed on the leading edge capture cells.

This work was supported by NASA Grant NAG-1-1174 and ESTEC AOP/WK/303284.

REFERENCES

1. Bradley, J. P.; Sandford, S. A.; and Walker, R. M.: Interplanetary dust particles. In Meteorites and the Early Solar System, eds. Kerridge, J. F.; and Matthews, M. S.; University of Arizona Press, 1988; pp. 861-895.
2. Brownlee, D. E.: Cosmic dust: collection and research. Ann. Rev. Earth Planet. Sci., 13, 1985, pp. 147-173.
3. Flynn, G. J.: Asteroids, Comets and Meteors III, 1989, pp. 59-62.
4. Flynn, G. J.: Survival of large micrometeorites on atmospheric entry: implications for their sources and the flux of cometary dust. Lunar Planet. Sci. XXII, 1991, pp. 393-394.
5. Zinner, E.; Kuczera, H.; and Pailer, N.: Simulation experiments for the chemical and isotopic measurements of interplanetary dust on LDEF. Lunar Planet. Sci. XIII, 1982, pp. 891-892.
6. Jessberger, E.; Kuczera, H.; Lange, G.; Sutton, S.; and Zinner, E.: Ion microprobe analyses of simulated LDEF impact residues. Lunar Planet. Sci. XVI, 1985, pp. 400-401.
7. Lange, G.; Eigner, S.; Igenbergs, E.; Jessberger, E. K.; Kuczera, H.; Maas, D.; Sutton, S.; Weishaupt, U.; and Zinner, E.: Ion microprobe sensitivities and their application to multielement analysis of LDEF impact residues. Lunar Planet. Sci. XVII, 1986, pp. 456-457.
8. Fraundorf, P.; Lindstrom, D.; Pailer, N.; Swan, P.; Walker, R.; and Zinner, E.: Rapid erosion of plastics in near-earth orbit and a means of prevention. Lunar Planet. Sci. XIV, 1983, pp. 205-206.
9. Fraundorf, P.; Lindstrom, D.; Pailer, N.; Sandford, S.; Swan, P.; Walker, R.; and Zinner, E.: Erosion of mylar and protection by thin metal films; AIAA Shuttle Environment and Operations Meeting; 1983; Paper 83-2636, pp. 131-137.
10. Fechtig, H.; Grün, E.; and Kissel, J.: Laboratory simulations. In Cosmic Dust, ed. McDonnell, J. A. M.; Wiley and Sons, New York, 1978; pp. 607-669.
11. Igenbergs, E.: Ein neuer Beschleuniger für die Simulation von Mikrometeoriten. Forschungsbericht, 1974, pp. BMFT-FBW 1974-03.
12. Stadermann, F.: Rare earth and trace element abundances in individual IDPs. Lunar Planet. Sci. XXII, 1991, pp. 1311-1312.
13. Zinner, E.; Tang, M.; and Anders, E.: Interstellar SiC in the Murchison and Murray meteorites: I sotopic composition of Ne, Xe, Si, C, and N. Geochim. Cosmochim. Acta, 53, 1989, pp. 3273-3290.